EUROPEAN ORGANIZATION FOR NUCLEAR RESEARCH

CERN – SL DIVISION

SL-Note-99-011 MS

Magnetic field calculations for the LEP spectrometer project

M. Sassowsky

Abstract

The LEP spectrometer aims at a precision measurement of the LEP beam energy. One of the key elements is the magnet that bends the beam. This note describes magnetic field calculations carried out to predict some of the magnetic properties of the spectrometer magnet. Furthermore, the study resulted in a modification of the pole shape in order to improve the transverse field homogeneity.

Geneva, Switzerland

March 15, 1999

Contents

List of Figures

List of Tables

1 Abstract

The LEP spectrometer [1] aims at a precision measurement of the LEP beam energy. One of the key elements is the magnet that bends the beam. This note describes magnetic field calculations carried out to predict some of the magnetic properties of the spectrometer magnet. Furthermore, the study resulted in a modification of the pole shape in order to improve the transverse field homogeneity.

2 Introduction

The aim of the LEP spectrometer project [1] is the precise measurement of the LEP beam energy. The basic measurement principle consists in bending the particle beam by a dipole magnet of bending power $\int B\,dl$. A beam of momentum p is deflected by the angle Θ:

$$\Theta = k \cdot \frac{\int B\,dl}{p} \qquad k = 0.2998\,\frac{\text{GeV/c}}{\text{Tm}} \tag{2.1}$$

As the spectrometer magnet is installed in the LEP accelerator, the bend angle is fixed and given by the machine layout. Measuring at different energies thus implies that the relative change of $\int B\,dl$ as a function of the beam energy must be known precisely. At the time of writing of this note, the magnet is being magnetically measured in the ISR tunnel to determine this quantity with high precision.

In view of the very tight schedule, it was decided in the early phase of the project to re-use an existing magnet design instead of developing a new dedicated magnet [2]. The LEP injection dipole MBI [5], [7] was chosen. The MBI magnets are C-magnets, the coil design is close to a racetrack shape.

The magnetic field inside an accelerator magnet, sufficiently far from the extremities, can be calculated with the help of a two dimensional field model. In this context ”two dimensional” means that the magnet is assumed to be infinitely long, so that the magnetic vector potential has only a Z component. For ”long magnets” (i.e. iron length large compared to aperture height and width) and for applications requiring not too high precision, this might already be a sufficient approximation of the properties of the integrated field. For sufficiently simple configurations, approximate estimates of some of the properties of the end field can be made using a longitudinal cut through the magnet. However only a full three dimensional field calculation can predict all three components of the end field properly.

3 Modelling considerations

Throughout this note the coordinate system shown below in Fig. 1 is adopted. Z is the longitudinal direction, $Z = 0$ corresponds to the magnet centre. X is the transverse direction; $X = 0$ mm is the nominal centre of the aperture, i.e. the nominal transverse beam position. Y is the vertical direction, $Y = 0$ is in the symmetry plane of the magnet.

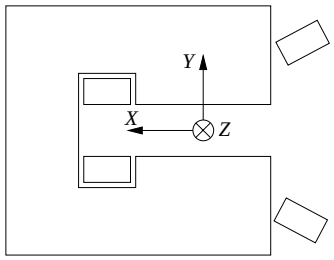

Figure 1: Coordinate system

3.1 Two dimensional field model

The 2D model is realised by the Opera-2D program [9] and is used to estimate properties in the centre of the magnet, sufficiently far away from the extremities. The simplest case, the magnet alone, is shown in Fig. 2. Only one half of the magnet is modelled because of the intrinsic symmetry, which is accounted for by normal boundary conditions on the X-axis.

The yoke uses material properties corresponding to Eq. 3.3, see the following chapter.

The coils are modelled as rectangular current carrying regions with the total current equal to the ampere-turns of the coil. The effect of the cooling holes and the spacing between the individual conductors can be neglected.

In the mid-plane an additional air region is used to create a fine and regular meshing. Outside the dimensions of the magnet yoke an air layer was included to minimise the influence of the outer boundary conditions on the results.

The triangular mesh is created by the automatic mesh generator of Opera-2D.

3.2 Three dimensional field model

3.2.1 Yoke

The yoke is built from 1.5 mm thick laminations of low carbon steel [8] stacked between two 30 mm thick massive end plates. To take into account the effect of the laminations, effective permeabilities for the directions parallel and perpendicular to the plane of the laminations have to be introduced. At the interface between a single lamination and the air gap between two laminations, the tangential component of the H field is continuous:

$$H_t = \frac{B_{air}}{\mu_0} = \frac{B_{steel}}{\mu_{steel}\mu_0} \tag{3.2}$$

The average tangential field B_t in the yoke is the weighted average between the field B_{steel} in the laminations and the field B_{air} in the air gaps between individual laminations, with the stacking factor s being the weight:

$$B_t = sB_{steel} + (1-s)\,B_{air} \tag{3.3}$$

Defining the effective tangential permeability μ_t by

$$B_t = \mu_t\mu_0 H_t \tag{3.4}$$

one obtains:

$$\mu_t = s\mu_{steel} + (1-s) \tag{3.5}$$

For common values of the stacking factor in the range between 0.96 and 0.99 and for usual steel permeabilities (several thousand), the second term $(1-s)$ can be safely neglected.

A similar consideration using the fact that the normal component of the B field at an air-iron interface is continuous leads to an expression for the effective normal permeability μ_n:

$$\mu_n = \left(\frac{s}{\mu_{steel}} + (1-s)\right)^{-1} \tag{3.6}$$

For the orders of magnitude of s and μ_{steel} given above, the second term $(1-s)$ dominates, so that the effective normal permeability is only weakly affected by the steel permeability, see Fig. 3. In particular, μ_n is small compared to μ_t and μ_{steel}, meaning that the B field lines are essentially parallel to the laminations – which is obvious from physical considerations. In Opera-3D [10], the effective normal and tangential permeabilities are calculated from the BH curve, the stacking factor and the orientation of the lamination [11].

The longitudinal fringe field originates from the end plates with the field direction essentially normal to the lamination plane. It is therefore important to include in the model the non-laminated end plate with an isotropic permeability equal to the steel permeability.

3.2.2 Coils

The coils of the MBI magnet are similar to racetrack coils, they are made of 3 circuits with 6 windings each. The coil heads are not identical, as one coil head contains the layer-to-layer transitions and the 6 coil tails for hydraulic and electrical connections. The model uses the BRICK and ARC primitives to model the shape of the coil heads identical to the actual shape on the non-connection side of the coil.

3.2.3 Meshing and potential types

The model was built using hexahedral meshes. The results using a mesh generated with the new automatic tetrahedral mesh generator introduced in version 7 of Opera-3D were found not to be accurate enough.

In the X-Y-plane the finest meshing was generated in the centre of the aperture and in the shim area, see Fig. 4. Several triangular regions (containing degenerate tetrahedral meshes) create transitions to the outside regions with a coarser mesh. An air layer outside the dimensions of the magnet yoke was included to minimise the influence of the outer boundary conditions on the results. The total number of meshes is about $250\,000$.

The model has only a length of 2060 mm, compared to the actual length of the magnet of 5750 mm, because it is only used to study end effects. The model assumes symmetry with respect to the X-Z-plane (normal boundary conditions at $Y = 0$), and to the X-Y-Plane (tangential boundary conditions at $Z = 0$). The latter symmetry condition is not fully correct because of the different shape of the coil heads at negative and positive Z. so the length of the half-yoke in the model is 1030 mm. In Z-direction the model consists of 5 layers. The co-ordinates, number of meshes and function of the layers are listed in Table 1.

All regions containing the coil, and the region between the pole faces, are reduced potential regions [12]; the yoke and part of the outer air regions are total potential regions. Care has been taken that the total potential regions and the reduced potential regions are topographically singly connected [12].

Fig. 5 shows a perspective view of the whole model and Fig. 6 a detailed view of the end region.

4 Results

4.1 Transverse homogeneity from 2D model

The transverse field homogeneity of the central field is determined by the pole shape. This shape, as used in the original MBI design [6], is sketched in Fig. 7. Note that the scale in Y-direction is highly exaggerated with respect to the X-direction. The main features are two asymmetrical shims and the slope of the pole face. The local transverse field homogeneity is shown as dashed line in Fig. 8.

While the slope creates a gradient in the centre of the aperture, the shims create an increase of the field off-centre, i.e. a sextupolar component. Removing the slope of the pole face, but leaving the shim geometry unchanged, leads to a much lower gradient of opposite sign in the centre of the aperture, see full line in Fig. 8. The remaining gradient is caused by the fact that the width and thickness of the two shims are different.

4.2 End field from 3D model

Fig. 9 shows the field in the Y-Z-plane at $X = 0$. The arrows indicate the direction of $\vec{B}$. Note that the size of the arrows is set constant and does not scale with the magnitude of the field. It can be seen that

the end field mainly originates in Z-direction from the end plates. The coil head cuts the Y-Z-plane at a right angle. The resulting field shape around the coil head is curl-like, as one expects.

The colour shading in Fig. 10 indicates the value of the magnitude $|\vec{B}|$ of the magnetic field in a logarithmic scale. The highest field levels can be found in the transition between laminated part of the magnet and the end plate. The latter "collects" all the end field from outside the magnet. The end field hardly penetrates into the laminated magnet body, because μ_n is small.

Fig. 11 shows the field in the X-Z-plane at $Y = 0$. The colour shading indicates the value of the magnitude $|\vec{B}|$ of the magnetic field. It can be seen that the field is asymmetric with respect to the beam axis, for $X < 0$ the field extends further into Z-direction than for positive X. The reason is the asymmetry of the coil head with respect to the pole centre: the smaller X, the larger the vertical distance between the upper and lower coil head, thus the larger the region from which the end field extends in Z-direction.

Fig. 12 shows the magnitude $|\vec{B}|$ of the magnetic field on the axis $X = 0$, $Y = 0$. The upper plot displays the proximity of the magnet in a linear scale, the lower plot a larger region in Z in a logarithmic scale. The attenuation by the end field screens (see chapter 4.5) is not included.

4.3 Transverse homogeneity of $\int B\,dl$

The pole shape of the original design would have led to a significant gradient component. This gradient has already been measured for the MBI's used in the LEP injection area (see Fig. 3 and Table 1 in [7]) and confirms these calculations. A transverse orbit motion of one millimetre would have caused a relative change of $\int B\,dl$ of 10^{-5}. For the spectrometer application a better transverse field homogeneity is highly desirable to avoid additional errors introduced by eventual orbit drifts in LEP. Consequently the punching die for the spectrometer magnet was modified and the magnet was built with parallel pole faces but unchanged shim geometry. The remaining gradient and sextupolar components are nearly compensated by the end field, as will be shown in this chapter.

To obtain the transverse homogeneity of the integrated field $\int B\,dl$, the contributions from the central field and the end field have to added. The upper left graph of Fig. 13 shows the transverse homogeneity of the end field at 44 GeV, as obtained from the 3D model. The integration region in longitudinal direction extends from Z=2675 mm to $Z = 3600$ mm, i.e. from 200 mm inside the yoke to 725 mm outside the yoke. Both the gradient at $X = 0$ and the pronounced sextupolar component are of opposite sign than those of the central field. The latter is shown in the middle left plot and is obtained by multiplying the local field from the 2D model with 5350 mm, i.e. yoke length minus twice 200 mm. Summing up both contributions yields the homogeneity of the total integrated field (lower left plot). While the sextupolar components cancel in a region of $X = \pm 25$ mm around the nominal beam position, a remaining gradient can be found. It corresponds to a relative variation of $+0.4$ ppm/mm.

Note that due to the sensitive cancellation of central field and end field contribution, artifacts caused by the finite mesh size of the two models can be seen as short range random variations.

The three plots on the right of Fig. 13 show the same quantities at 100 GeV. The sextupolar components cancel; the gradient changes its sign with respect to 44 GeV and corresponds to a relative variation of -1.0 ppm/mm.

4.4 Influence of the girder on the central field

The mechanical stability of the original MBI design was considered to be not sufficient [2], so a dedicated support structure called girder was built. As the permeability of the construction steel used for the girder is comparable to that of the magnet steel [2], the influence of the girder on the central field was investigated. The 2D model was extended and the geometry of the girder [3] included. As the girder breaks the up-down-symmetry, the full magnet was modelled.

The resulting field line plot is shown in Fig. 14. The girder attracts part of the stray field and acts as an additional return yoke. The latter fact can be seen more clearly when displaying only those field lines that actually pass through the girder (Fig. 15).

The homogeneity curves with and without girder, and the difference ΔB between them, are shown in Fig. 16. While the magnitude of the field is increased by about $5 \cdot 10^{-6}$ T at 100 GeV, the transverse homogeneneity is virtually unchanged. The binning effect in the plot of ΔB vs. X is caused by the limited number of digits (6) that the program [9] uses to output the results.

The fact that the girder breaks the symmetry leads to a tiny transverse field component in the mid-plane of the magnet. Its magnitude at $X = 0$ is about 10^{-5} T at the center of the aperture (see Fig. 17) and produces a tilt of the magnetic field direction of $4.5 \cdot 10^{-2}$ mrad. This is equivalent to a mechanical tilt of 0.02 mm over the width of the magnet and thus appears negligible.

The magnetic measurements will be carried out while the magnet is already mounted to the girder, so all in all the influence of the girder on the central field was considered to be negligible.

To avoid a disturbance of the end field, the total length of the girder is 5550 mm [3], i.e. 200 mm less than the length of the yoke.

4.5 End field screens

As can be seen from Fig. 12, the end field has no defined cut off. Far away from the magnet it might thus be modified by the environment, which is different during the magnetic measurements compared to the operation in the LEP tunnel. It is thus desirable to cut off the field at a certain distance, so that the quantity $\int B\, dl$ determined by magnetic measurements is the same as the $\int B\, dl$ experienced by the beam. This cut off can be achieved by a shield of μ-metal wrapped around the vacuum pipe.

A 3D model was created to estimate the attenuation factor. To avoid modelling the magnet **and** the shield, leading to a complex mesh, only the shield was modelled (see Fig. 18) and placed into a homogeneous field with a magnitude comparable to the value obtained from the 3D model. A very conservative value of 5000 for the permeability of the μ-metal was used, taking a margin for an eventual deterioration of the magnetic properties by the mechanical treatment that is necessary to wrap the sheets around the vacuum pipe.

Fig. 19 shows the magnitude of $\vec{B}$ as a function of Z, normalised to the outside field. The distance between end plate and the beginning of the screen was chosen to be 500 mm. Using three layers of 0.2 mm thick sheets, as assumed in the model, an attenuation factor of 10 should be reached.

5 Conclusion

Magnetic field calculations were carried out to investigate the magnetic properties of the spectrometer magnet. As a result of this study the MBI spectrometer magnet was built with a modified pole shape with respect to the original MBI design leading to a significantly better transverse homogeneity of $\int B\, dl$. The influence of the girder on the central field appears negligible. μ-metal shields have been designed to attenuate the far end fields by at least a factor of 10.

References

[1] The LEP Spectrometer Project, LEP Spectrometer Working Group, CERN-SL note in preparation

[2] Private Communication G. de Rijk, CERN SL division

[3] Private Communication W. Weterings, CERN SL division

[4] Private Communication B. Dehning, CERN SL division

[5] Technical specification for the supply of of the MBI dipole cores for LEP 200, CERN AT-MA/90-36

[6] Drawing 02-P81-D1, TESLA Engineering Limited, Storrington, Sussex RH20 3EA, England

[7] Mésures magnetiques des aimants dipolaires d'injection du LEP 200, CERN AT-MA/CR/PV/fm-1403 Note technique 92-32

[8] Magnetil BC steel, Cockerill Sambre, Seraing, Belgium

[9] Opera-2D version 1.6, Vector Fields Limited, 24 Bankside, Kidlington, Oxford OX5 1JE, England

[10] Opera-3D version 7.005, Vector Fields Limited, 24 Bankside, Kidlington, Oxford OX5 1JE, England

[11] Opera-3D applications notes, VF-01-98-X6

[12] Opera-3D user guide, VF-01-98-D2, Chapter 2

Appendix

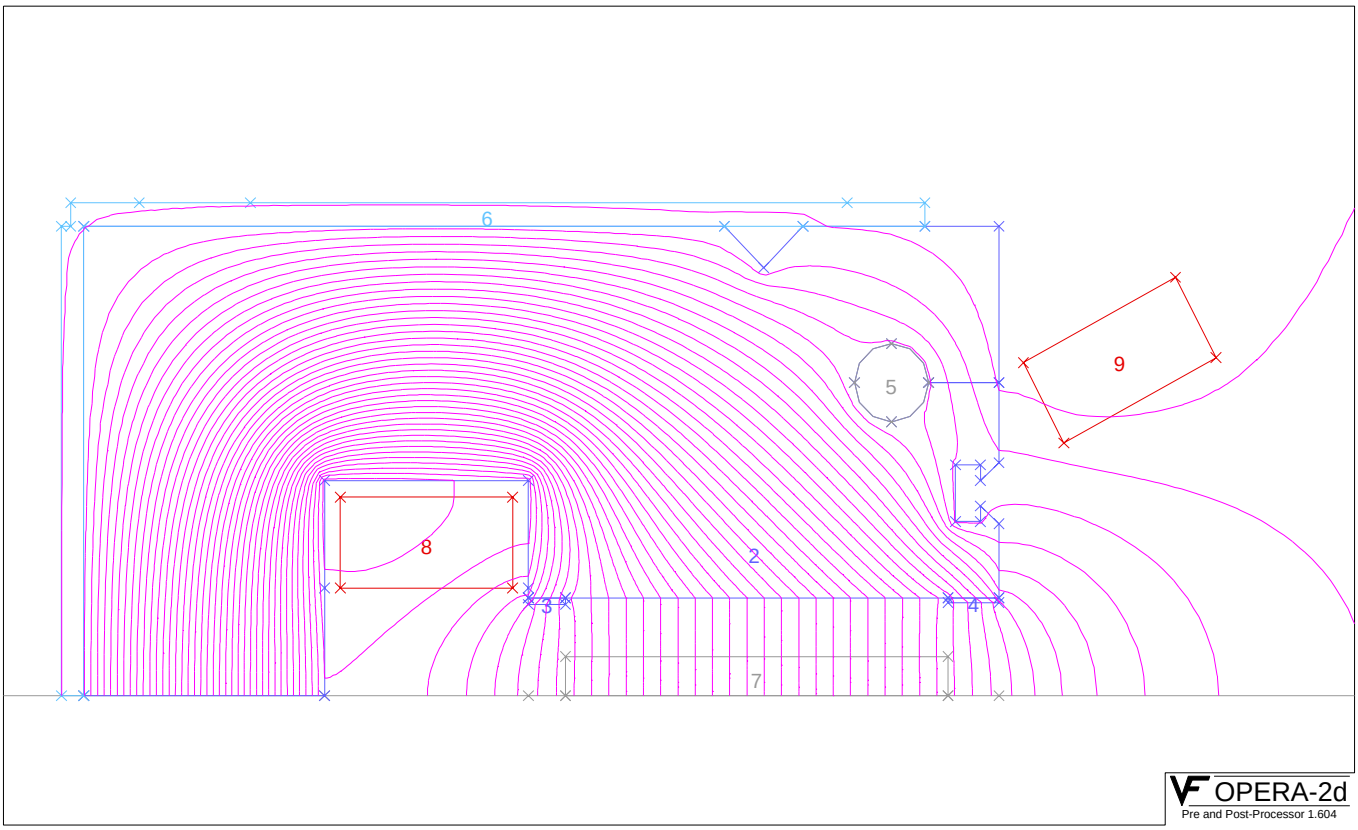

Figure 2: Two dimensional model

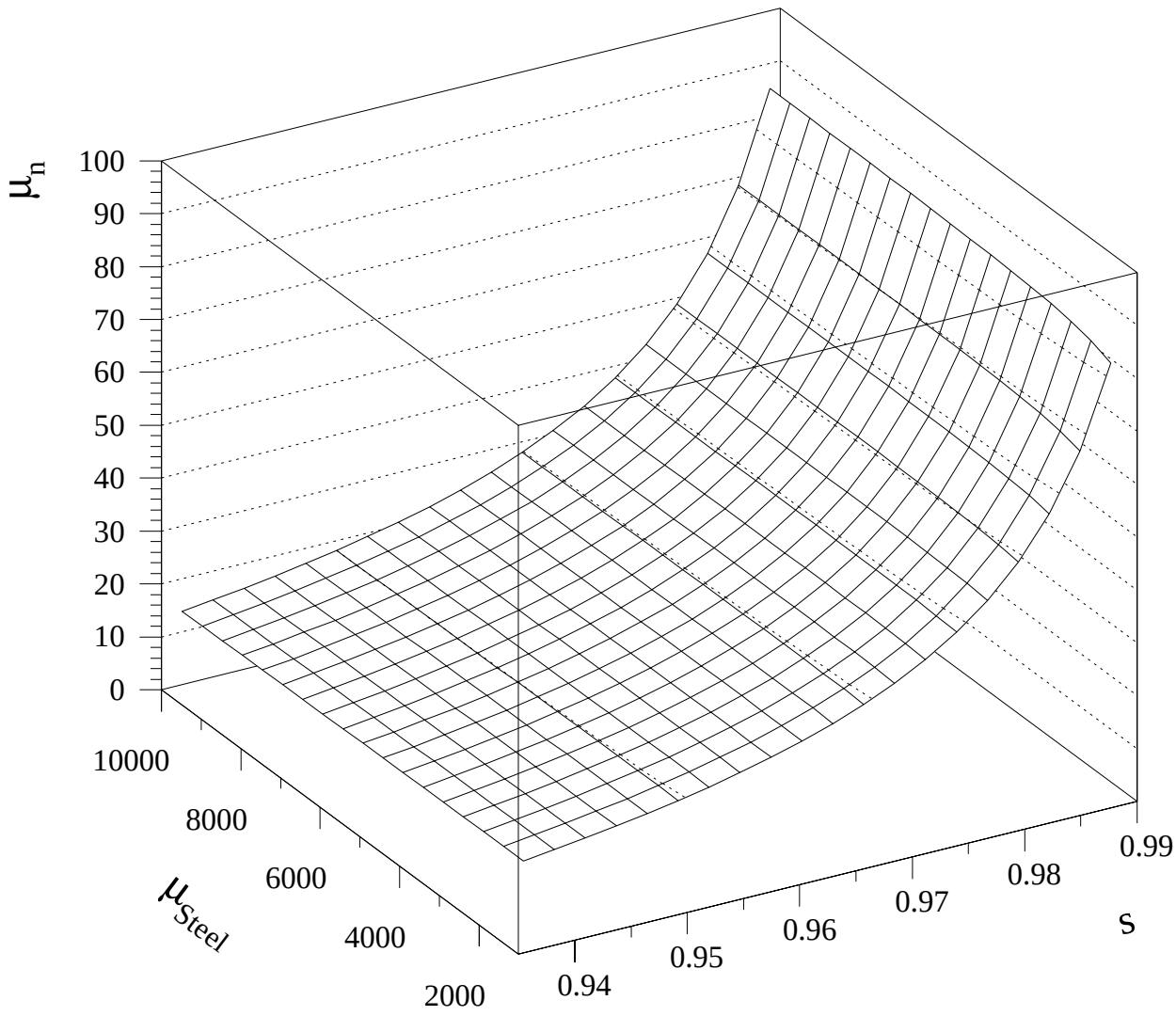

Figure 3: Effective normal permability μ_n as a function of stacking factor s and steel permeability μ_{steel}

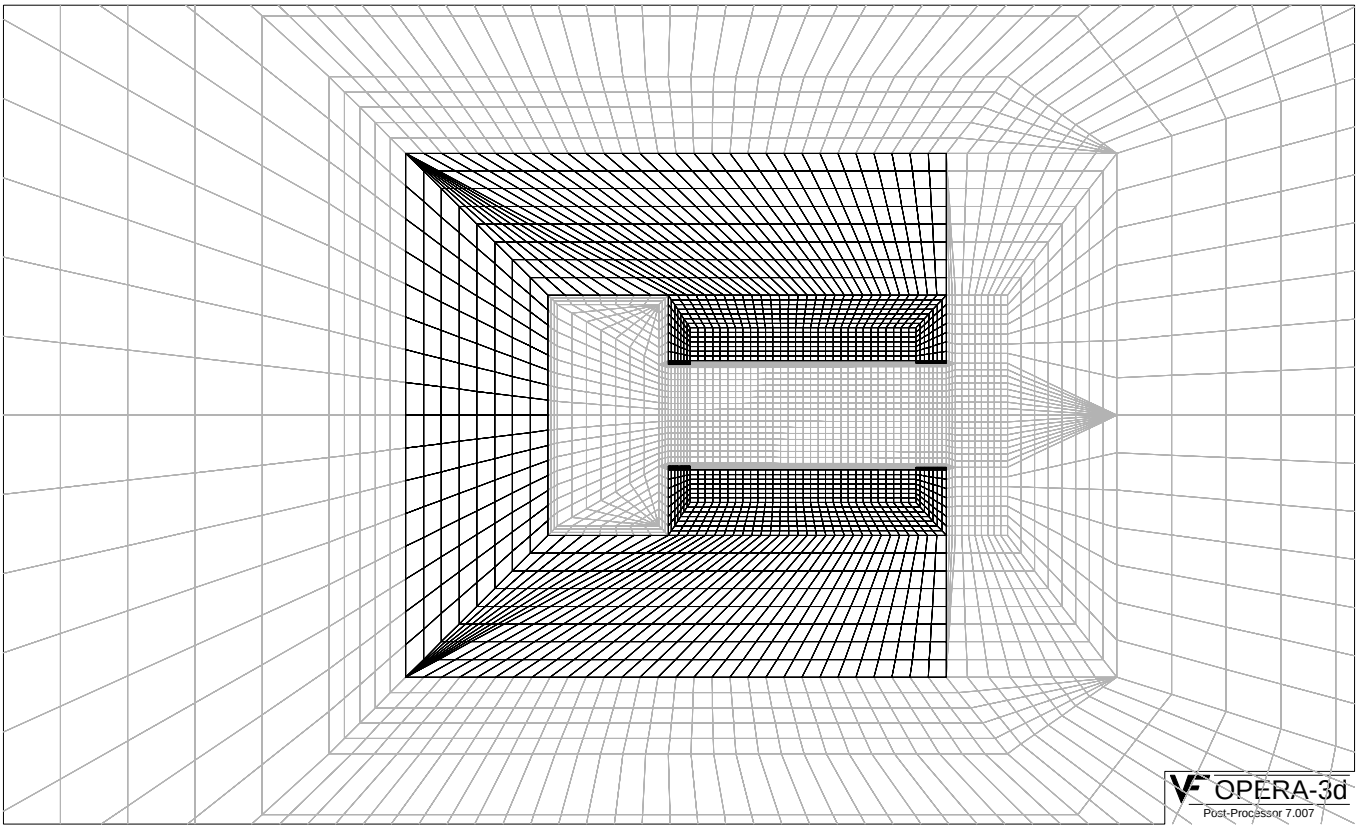

Figure 4: Part of mesh in the X-Y-plane of the three dimensional model, showing aperture, yoke (black) and part of outer air region

Layer Number	Z_{min} [mm]	Z_{max} [mm]	Number of meshes	Description
1	1845	2745	10	Central part of magnet
2	2745	2845	20	Finer meshing as transition to end plate region
3	2845	2875	10	End plate
4	2875	3075	10	Near end field
5	3075	5075	40	Far end field, coarser meshing

Table 1: Z-layers of the three dimensional model

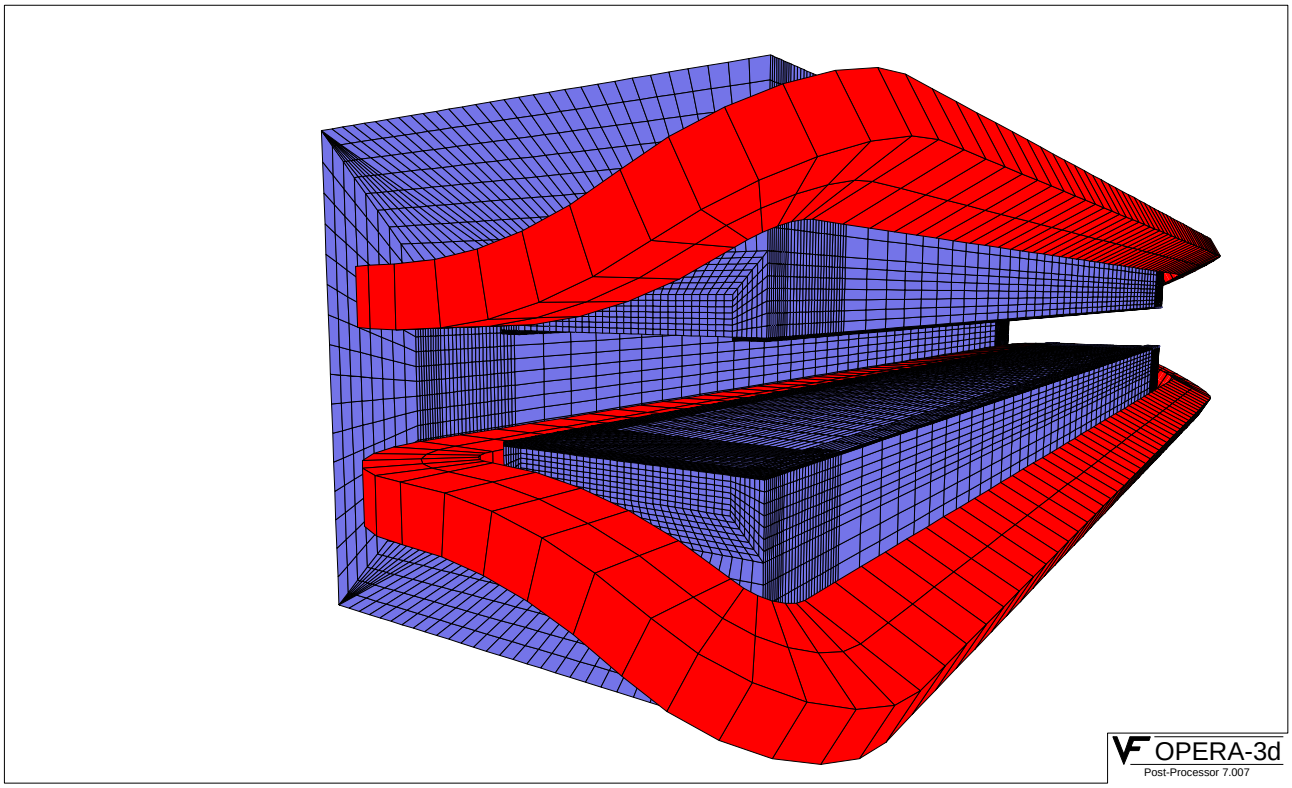

Figure 5: Perspective view of the three dimensional model

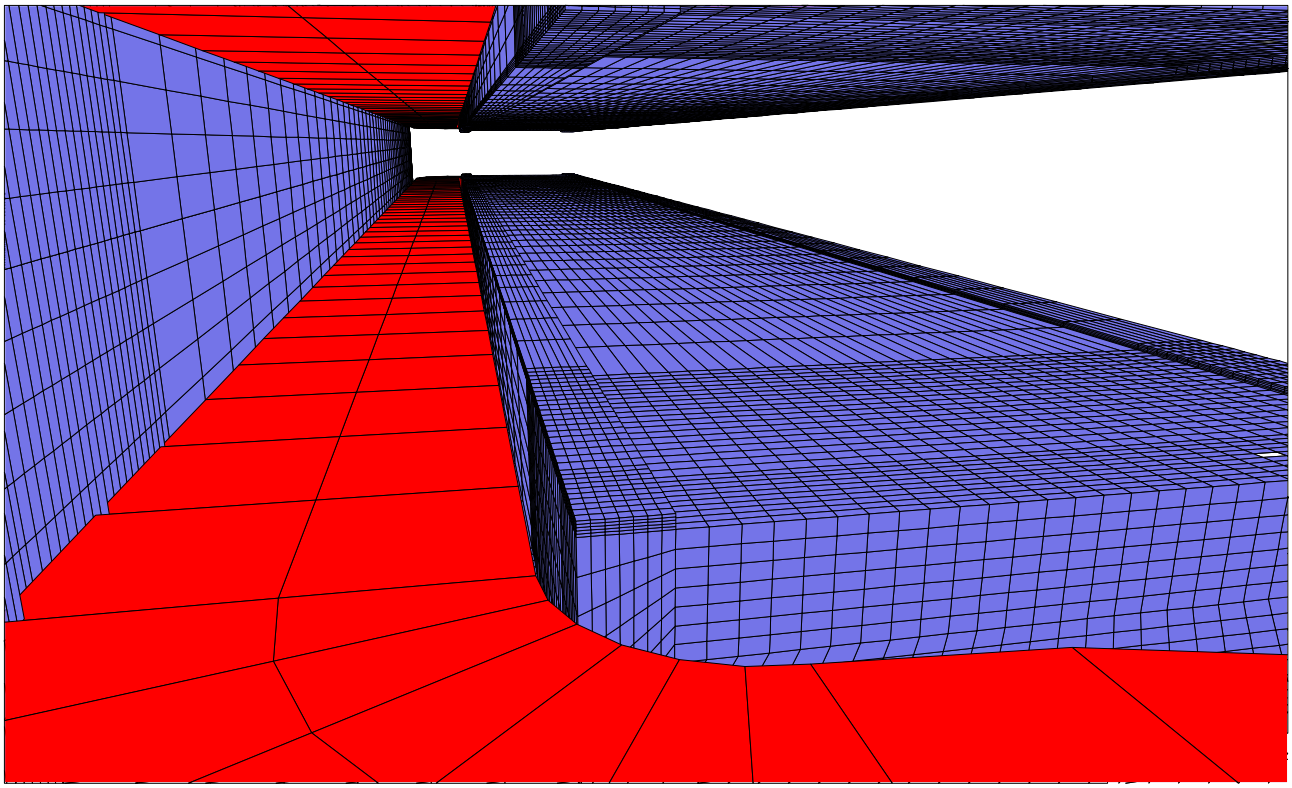

Figure 6: End of yoke region of the three dimensional model

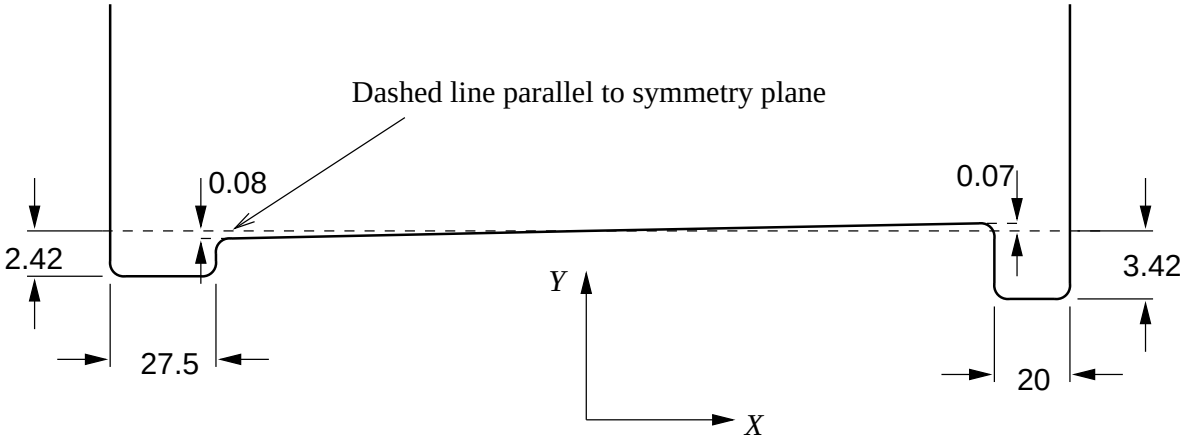

Figure 7: Poleshape of original MBI magnet

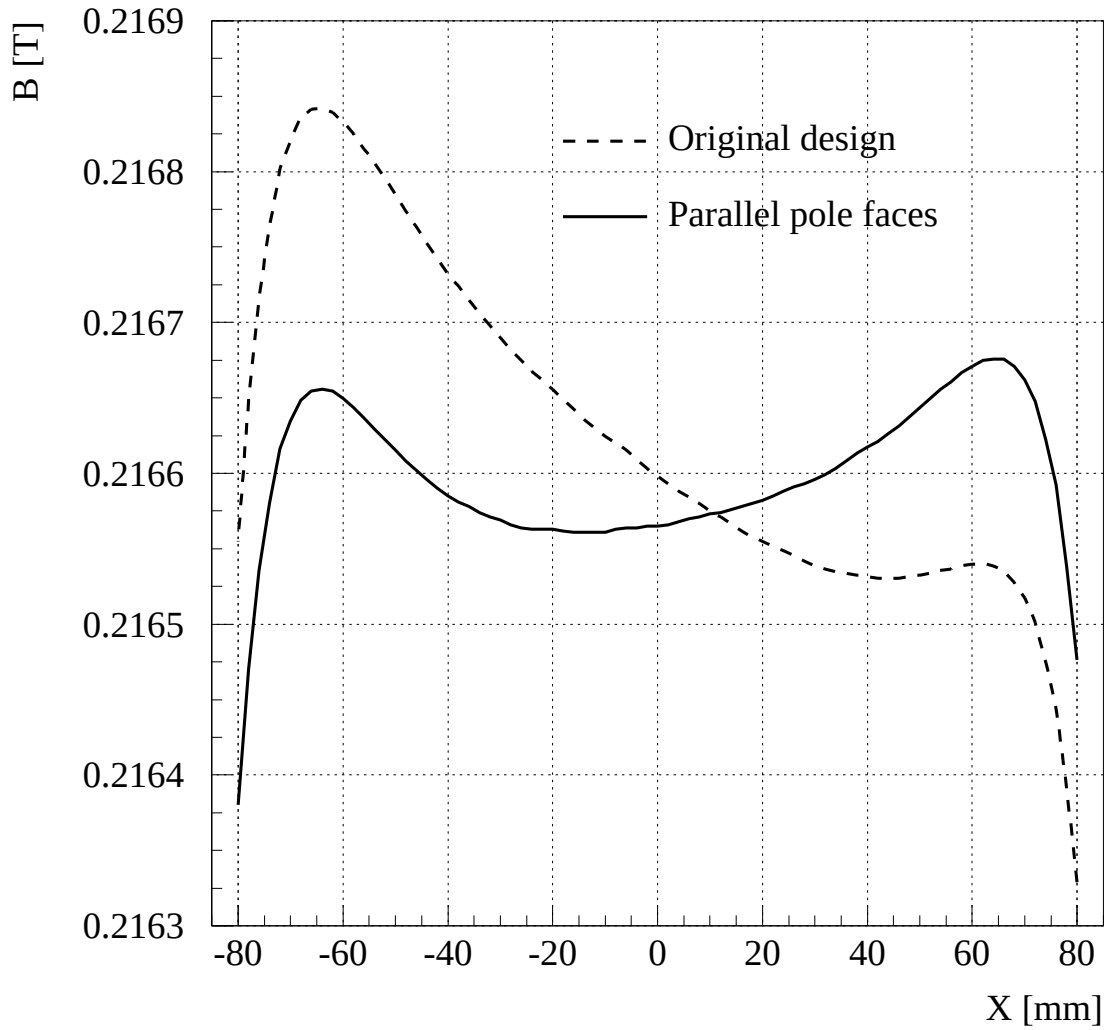

Figure 8: Transverse field homogeneity from 2D model

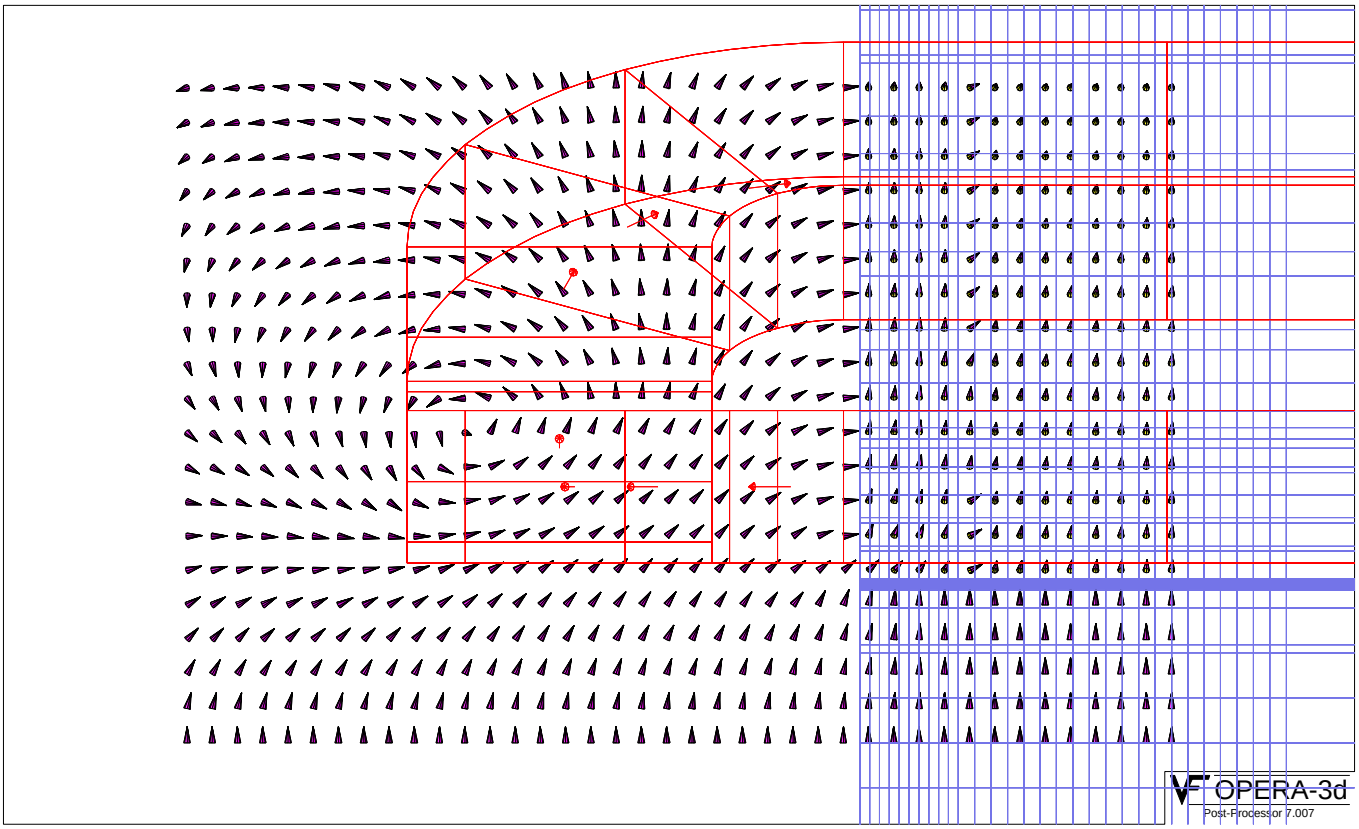

Figure 9: Field direction in the Y-Z-plane at $X = 0$

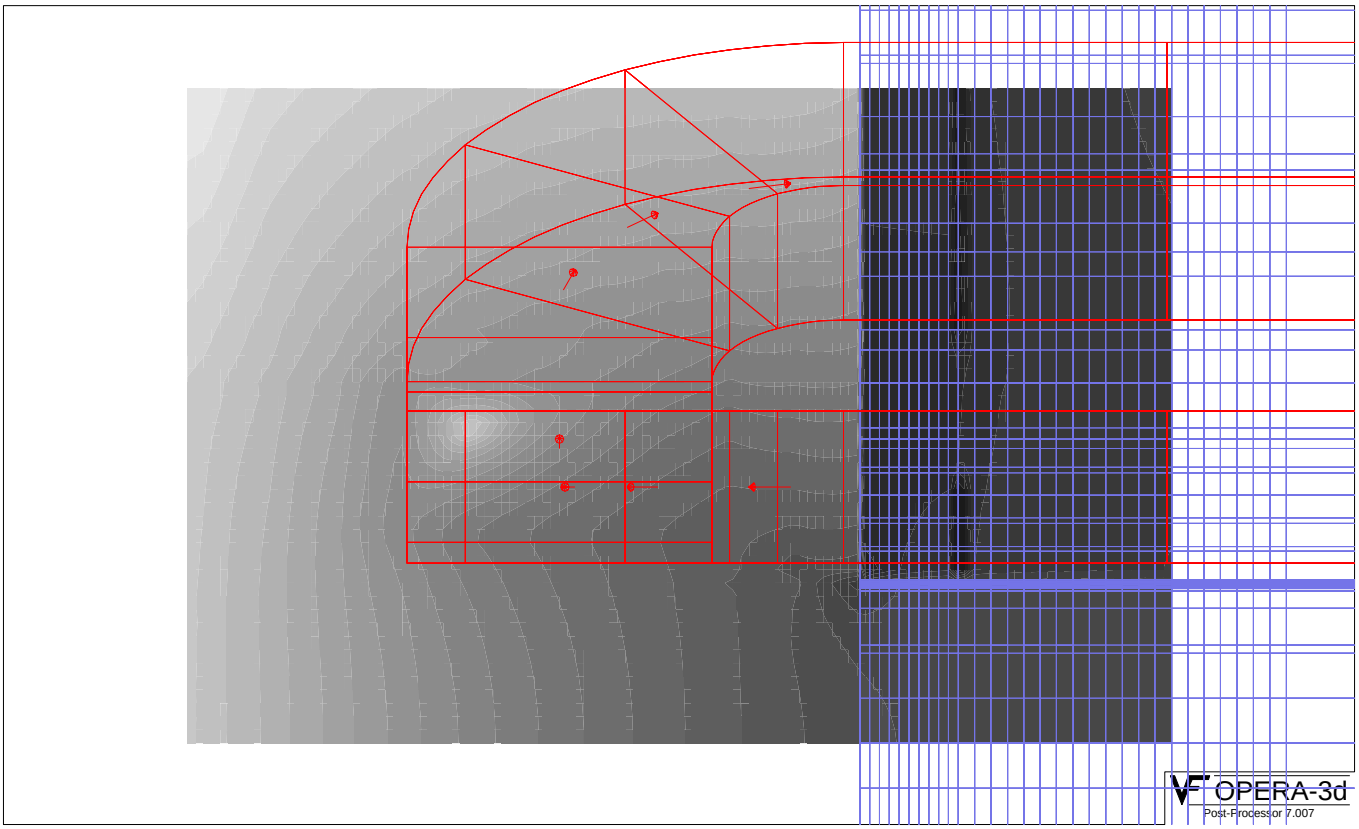

Figure 10: Field strength in the Y-Z-plane at $X = 0$

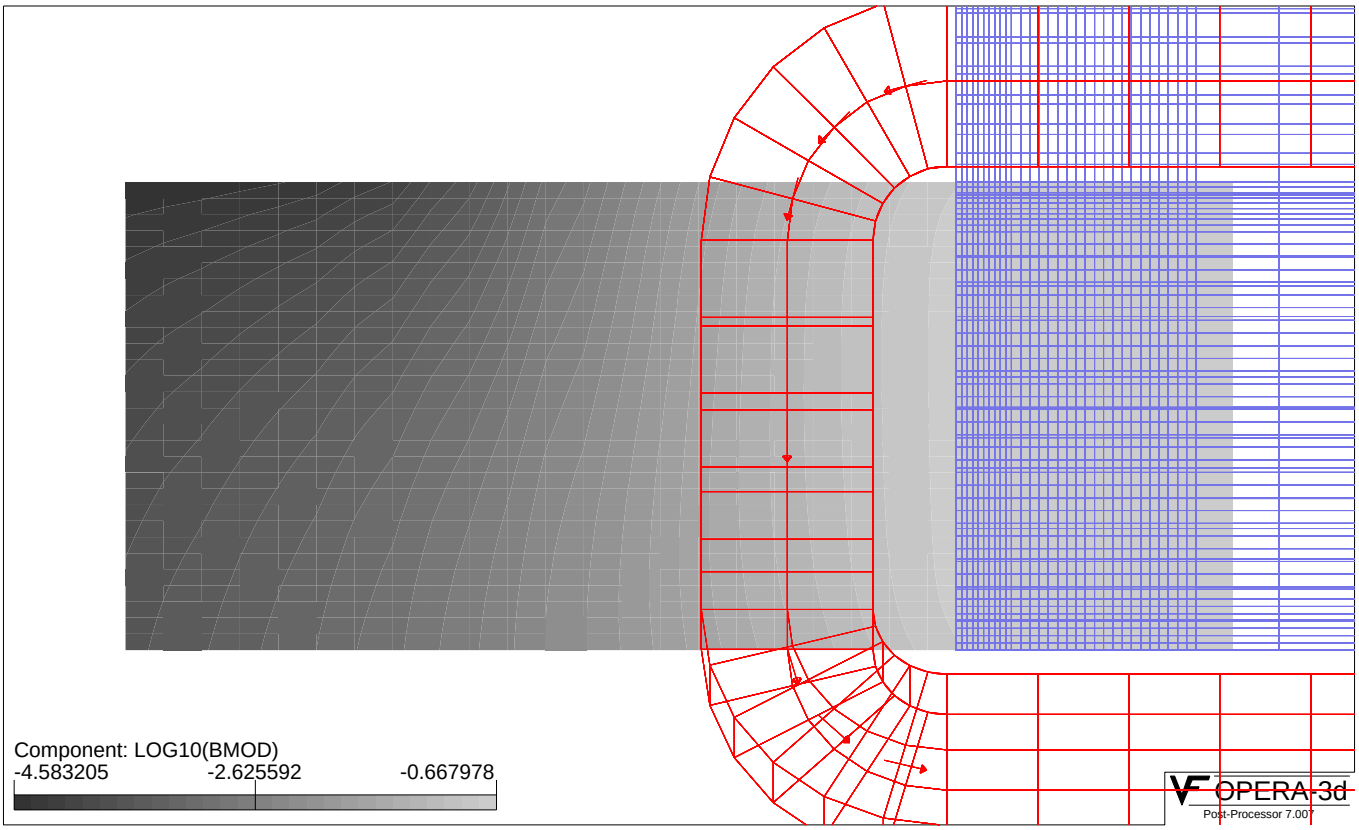

Figure 11: Field in the X-Z-plane at $Y = 0$

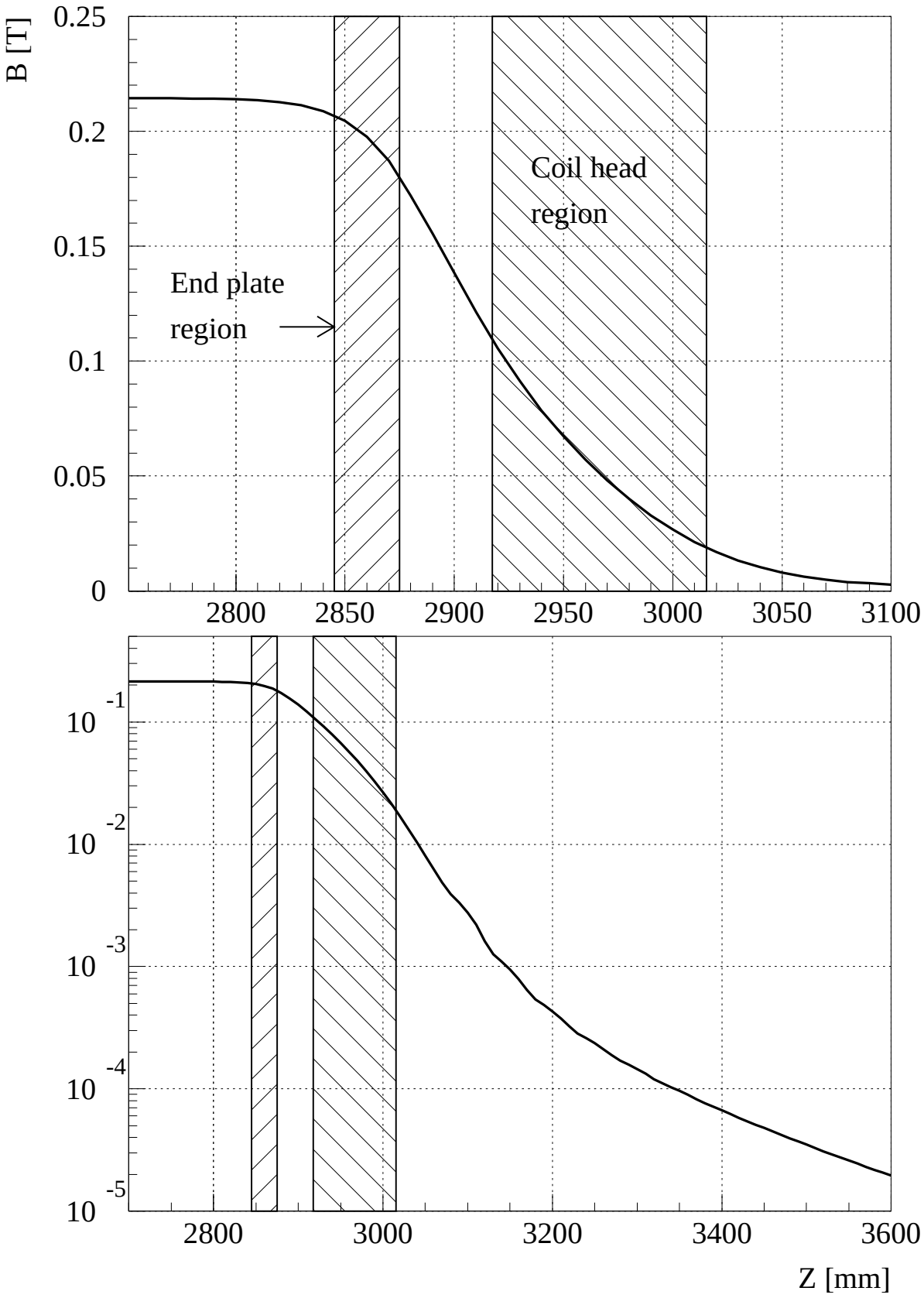

Figure 12: Magnitude $|\vec{B}|$ of the magnetic field on the axis $X = 0, Y = 0$

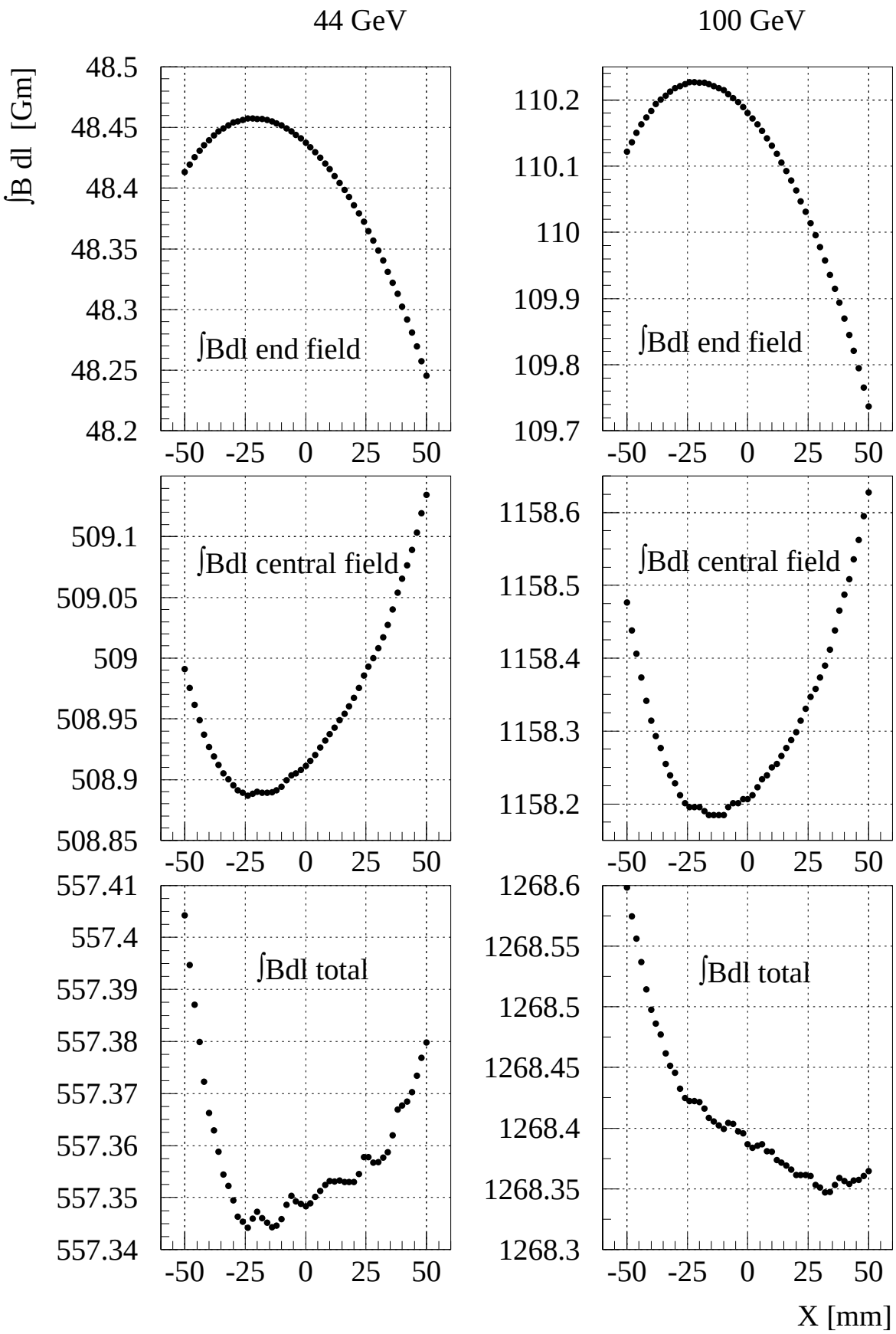

Figure 13: Transverse homogeneity of central-, end- and total field

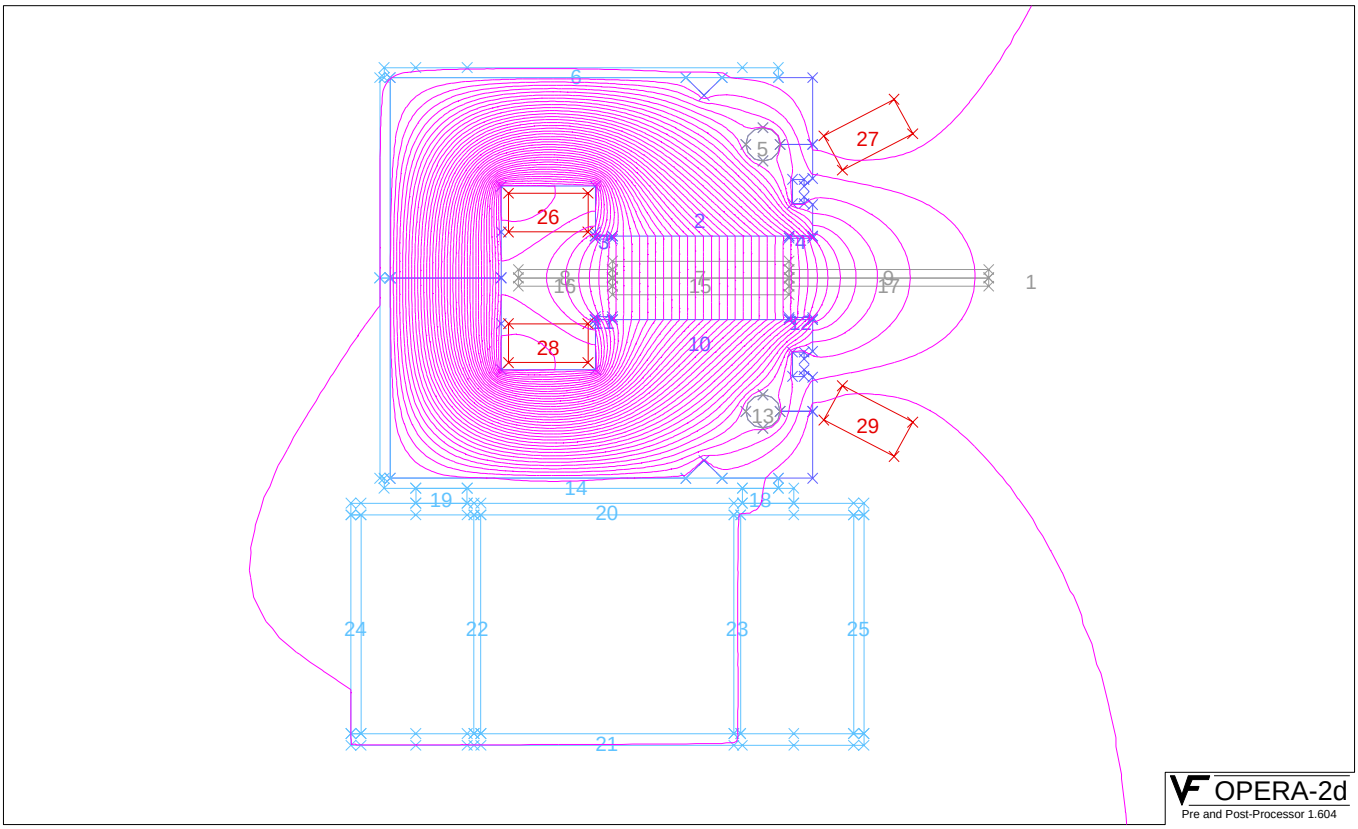

Figure 14: Field lines in MBI on the girder

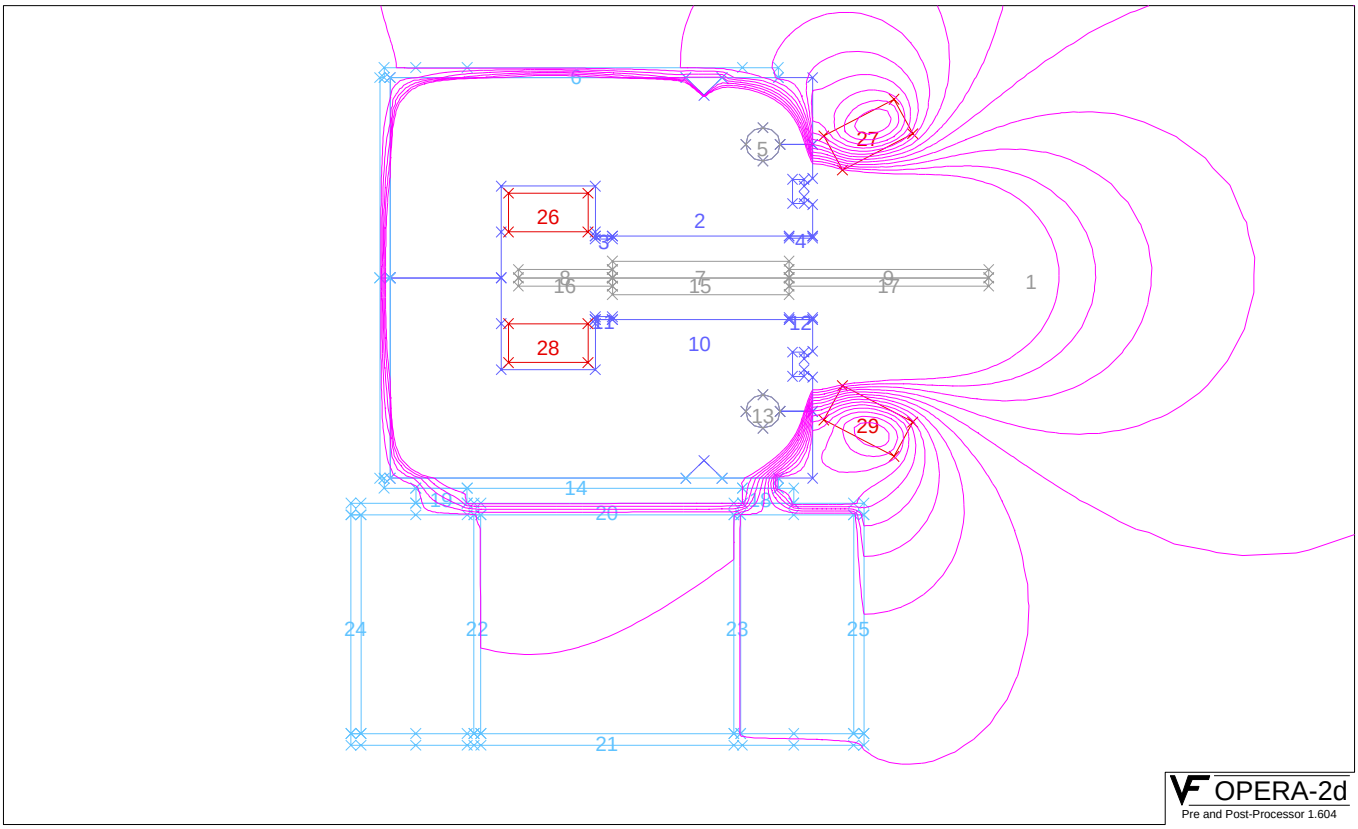

Figure 15: Field lines that pass the girder

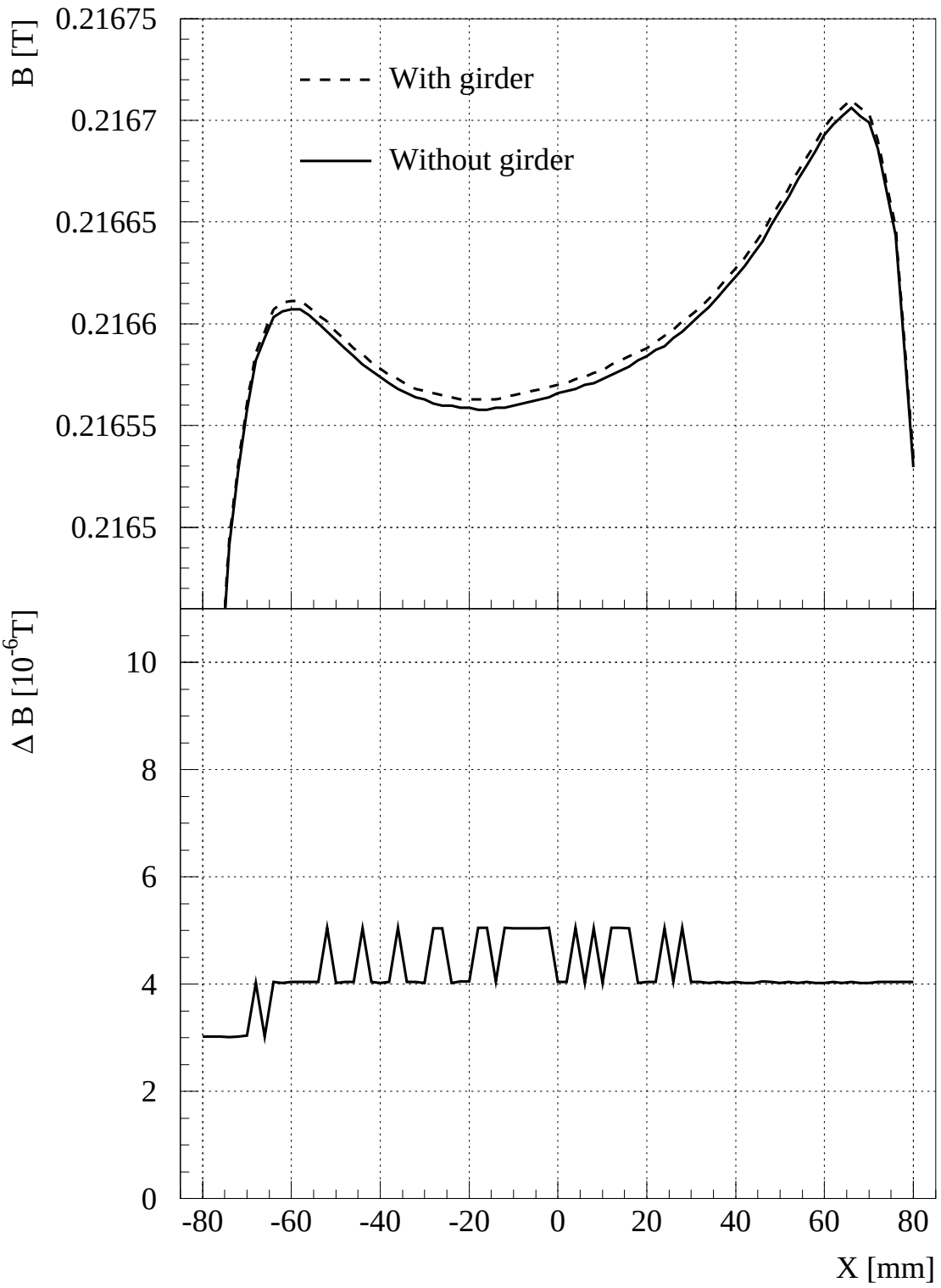

Figure 16: Homogeneity curves with and without girder, and difference ΔB between them, as a function of transverse position

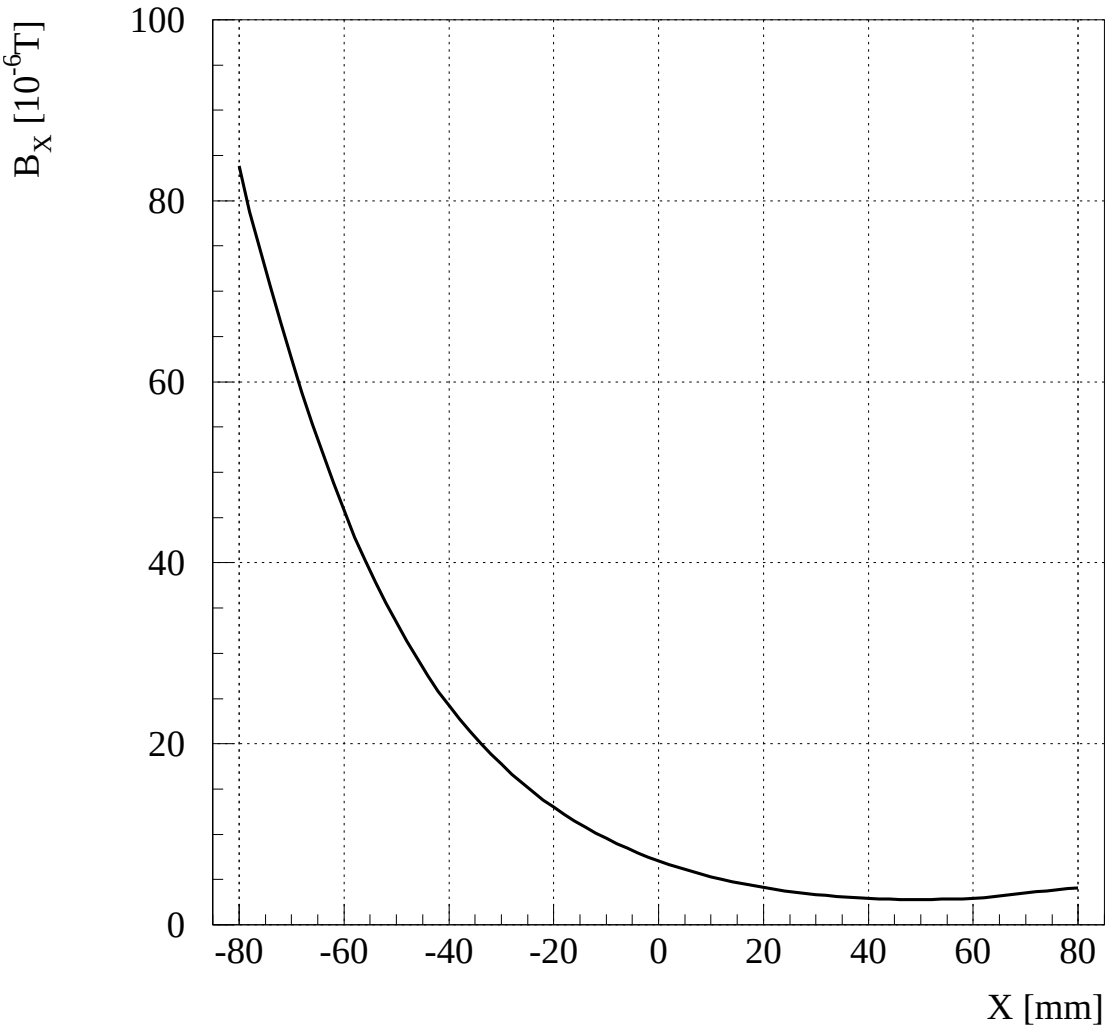

Figure 17: Transverse field component caused by the girder

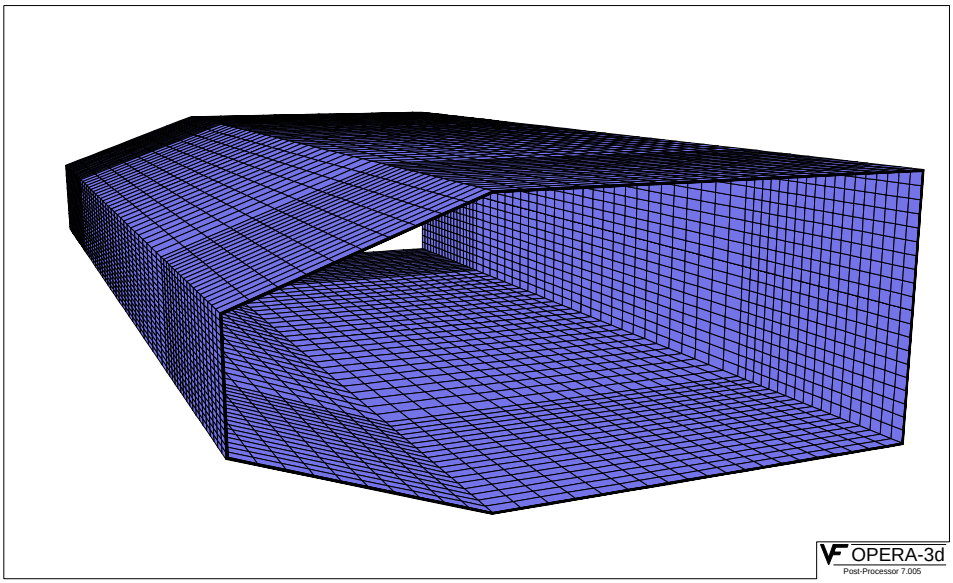

Figure 18: Perspective view of the end field screen

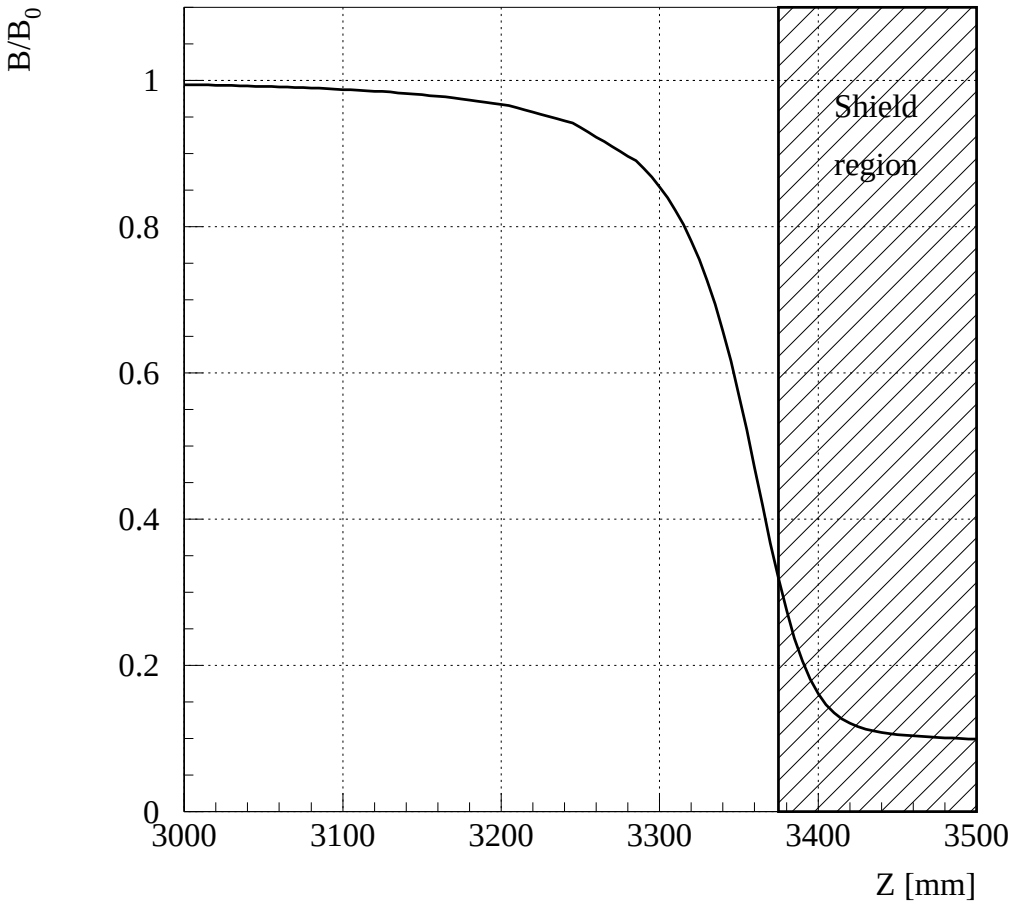

Figure 19: Field attenuation by the end field screen